THE ASTROPHYSICAL JOURNAL, 330:254–263, 1988 July 1

THE EVOLUTION OF THE RADIO EMISSION FROM KEPLER'S SUPERNOVA REMNANT

JOHN R. DICKEL,[1] ROBERT SAULT,[1] RICHARD G. ARENDT,[1] YUTAKA MATSUI,[2] AND KIRK T. KORISTA[1]
Received 1987 September 28; accepted 1987 December 15

ABSTRACT

High-resolution radio maps of Kepler's Supernova remnant (SNR) using all four arrays of the VLA have been obtained at wavelengths of 20 and 6 cm. They show the complete structure of the remnant; all features are resolved with sizes greater than about 2″, and the relative brightness of the smooth component near the center is about $\frac{1}{4}$ the brightness of the rim. The results have been compared with earlier more limited data (Matsui *et al.*) to measure changes in the remnant over a 4 yr time span. The SNR is expanding with a mean rate of $R \propto t^{0.50}$ with considerable variations around the shell. Values range from $R \propto t^{0.35}$ on the bright northern rim at $R \propto t^{0.65}$ on the eastern part of the shell. The measurements are consistent with expansion into a variable circumstellar medium.

Subject headings: nebulae: individual (Kepler's supernova) — nebulae: supernova remnants — radio sources: general

I. INTRODUCTION

As a young supernova remnant (SNR) expands, a forward shock will move outward into the surrounding medium and a reverse shock will move back into the ejected material. At early times, the expansion will be controlled by the density distribution in the outer atmosphere of the initial star and the so-called "expansion parameter," x, where radius is proportional to time^x, can be calculated from the stellar parameters (Chevalier 1982). After the expanding material has swept up about 8 times the ejected mass and the reverse shock has passed through the ejectum the expansion will act like outward flow from a point explosion. This later phase can be represented by a similarity solution in which the expansion parameter is 0.4 (e.g., Sedov 1959).

Although we have a general picture, full understanding requires repeated observations with high sensitivity of all scale sizes within several remnants to determine their actual changes with time. SNR produce radiation in all wavelength ranges but, to date, only radio and optical observations offer both the resolution and time baseline to look at detailed structure and its variations. Expansion has been measured at both optical and radio wavelengths in Cas A and Tycho's SNR. Cas A, probably the remnant of a Type II SN in 1658 (van den Bergh and Kamper 1983), shows very irregular motions but is expanding within the range expected for a young SNR (van den Bergh and Kamper 1983; Bell 1977; Dickel and Greisen 1979; Tuffs 1984). Tycho's (1572) SNR is expanding definitely faster than the Sedov rate by a small amount (Strom, Goss, and Shaver 1982; Tan and Gull 1985; Kamper and van den Bergh 1978). The second youngest SNR known in the Milky Way, the remains of the Type I event recorded by Kepler in 1604, should show expansion and may differ from Tycho because of its relatively high Galactic latitude and direction toward the center of the Galaxy. Its distance is quite uncertain but is generally adopted as 5 kpc (see, e.g., White and Long 1983). Very few optical filaments are visible and measurements of their proper motions indicate only very slow expansion (Kamper and van den Bergh 1978). However, these filaments are likely to be features which have recently been struck by the forward shock and have not yet acquired significant momentum from the expanding material. It is thus important to measure the expansion of the radio shell of Kepler's SNR. It is a particularly good candidate for study with the VLA.[3] The remnant is small enough, about 200″ in diameter, so that the smoothly distributed emission can be recorded using the short spacing D array of the instrument yet the smallest features also appear to be fully resolved by the extended A array.

First-epoch maps at wavelengths of 20 and 6 cm were made in 1981–1982 (henceforth called 1981 maps) with combined A and C arrays of the VLA by Matsui *et al.* (1984, hereafter MLDG). MLDG showed the detailed brightness and polarization distributions of the object. This paper reports a repeat of the above observations in 1985, 1% of the total age of the remnant later. The new results also include data from the B and D arrays of the VLA so that the relative brightnesses of the smooth and fine-scale structures could be better compared for a complete brightness distribution. The synchrotron radio emission appears to come from a complete but somewhat irregular thick shell while the optical radiation is line emission generally arising in a limited number of filaments near the edge of the object (see, e.g., MLDG). The relativistic particle acceleration and magnetic field enhancement needed to produce the radio emission can come from shocks and from eddy motion at Rayleigh-Taylor unstable interfaces between the ejected and swept-up material (Gull 1973). The thickness of the shell and the observed brightness fluctuations can be caused by multiple shocks and interfaces resulting from small-scale clumping in the circumstellar medium (Dickel, Jones, and Eilek 1987). In § II of the paper the observations and data reduction are described. Analysis of the improved maps and the two-epoch comparisons are in § III. Discussion follows in § IV.

II. OBSERVATIONS AND DATA REDUCTION

The observations at both epochs are listed in Table 1 and the characteristics of the maps are given in Table 2. All maps were made more than twice the size of the SNR so that deconvolutions and comparisons of the fast Fourier transformed data could be made without problems from aliasing. They were also

[1] Astronomy Department, University of Illinois.
[2] Physics and Astronomy Department, Northwestern University.
[3] The VLA of the National Radio Astronomy Observatory is operated by Associated Universities, Inc., under contract with the National Science Foundation.

TABLE 1

OBSERVATIONS

Date	Array	Frequencies (MHz)	Bandwidth (MHz)	Total On-Source Integration (minutes)
		1984–1985		
1984 Aug 10	D	1465, 1515 4835, 4885	50 50	55 81
1985 Feb 4	A	1407, 1465 4816, 4866	12.5 12.5	80 171
1985 May 5.....	B	1452, 1502 4823, 4873	25 25	88 163
1985 Jul 15	C	1465, 1515 4835, 4885	50 50	78 170
		1981–1982		
1981 Feb 22	A	1407 4866	12.5 12.5	80 154
1982 Jan 4	C	1465 4885	50 50	80 148

constructed with uniform weighting of the spatial-frequency visibilities so that fine structure could be brought out; this resulted in measured noise levels which were higher than predicted from the system noise alone. Despite the IAU resolution supporting the use of J2000 coordinates, the 1985 data were recorded in the B1950 system to maintain consistency with the earlier observations.

a) Maps from the Complete Data Set

The data obtained in 1984–1985 from all four arrays were combined directly to make the complete maps. Although the D array observations were earlier in time than the others, the D array covered the shortest innermost spacings which should register negligible variations over the given time interval. Because of the southern declination of the source, even with full coverage from all arrays of the VLA, the beams are very elliptical with major axes in a nearly north-south direction.

At 20 cm, a zero-spacing flux density of 17 Jy was added to the data before construction of the map to account for the total emission from the SNR. Information at other short spacings is still missing but the reasonably small diameter of the source (about 200″) should result in little variation in the amplitudes of the visibilities at spacings shorter than about 200 m, which is well covered by the tight D array of the VLA. Thus the observed brightness distributions should be a good representation of the emission from Kepler's SNR. Further processing to improve the visibility of features on the map was done using maximum-entropy deconvolution. The final map is displayed in Figure 1 (Plate 8). This map has not been corrected for the response of the primary beams of the VLA antennas which reduce the brightness by $\frac{1}{2}$% at the outer edge of the SNR.

At 6 cm, the extremely large map required to fully utilize the available resolution was made on the Cray X-MP of the National Center for Supercomputer Applications at the University of Illinois.[4] Deconvolution was again done with maximum entropy. In this case the original map was constructed without a zero-spacing flux density and the MEM routine was given an estimate of 6 Jy for the integrated flux density. The final solution gave 6.3 Jy. At this resolution the surface brightness was so low that the data were near the noise level and the maximum entropy analysis made little improvement to the visibility of features on the map. The solution, however, does show that essentially all of the flux density of the source is being recorded and the missing short spacings do not contain significant information. The final map is presented in Figure 2 (Plate 9). This map was also uncorrected for the primary-beam pattern; in this case the brightness at the outermost edge of the remnant is 6% lower than it should be if corrected.

Polarization maps were also constructed from these new complete data sets. Because of the low surface brightness of the polarized component which is only about 5% of the total surface brightness, the 6 cm results were not significantly improved over those presented by MLDG, who found a Faraday rotation which was less than 32 radian m^{-2} everywhere in the remnant, a radial orientation of the magnetic field in the shell, and very small depolarization between 6 and 20 cm. Only the new results of 20 cm will be considered here. The maps of the Q and U polarized intensities were processed with an AIPS routine UTESS which maximizes the emptiness of a map and allows negative values. The maximum emptiness is determined by counting the number of cells which are within the noise level of zero and maximizing a function which measures this number (T. Cornwell, private communication). A gray-scale map of the polarized intensity formed from the component maps is shown superposed on the total-intensity contours in Figure 3 (Plate 10) and the electric vectors are plotted in Figure 4. In order to be seen, only every fourth vector has been plotted. An enlargement of the northwestern corner of the remnant with every vector shown is presented in Figure 5. This reveals that the detectable polarization structure is smoother than the resolution so that Figure 4 is sufficient to show the overall polarization of Kepler's SNR.

[4] The NCSA is operated by the University of Illinois under contract with the National Science Foundation.

TABLE 2

2 MAPS

Purpose	Wavelength (cm)	Beam HPBW (arcsec)	Beam P.A. (deg)	Pixel Spacing (arcsec)	Measured RMS Noise (mJy)	Mean Date
1981 comparison ...	20	2.26 × 1.23	−21	0.5	0.07	1981 Jul 30
	6	1.03 × 0.56	−14	0.25	0.04	
1985 comparison ...	20	2.26 × 1.23	−21	0.5	0.07	1985 Apr 25
	6	1.03 × 0.56	−14	0.25	0.04	
1985 all data	20	2.72 × 1.65	0°	0.5	0.03	1985 Feb 22
	6	0.93 × 0.51	0°	0.15(R.A.) 0.3 (decl.)	0.01	

PLATE 8

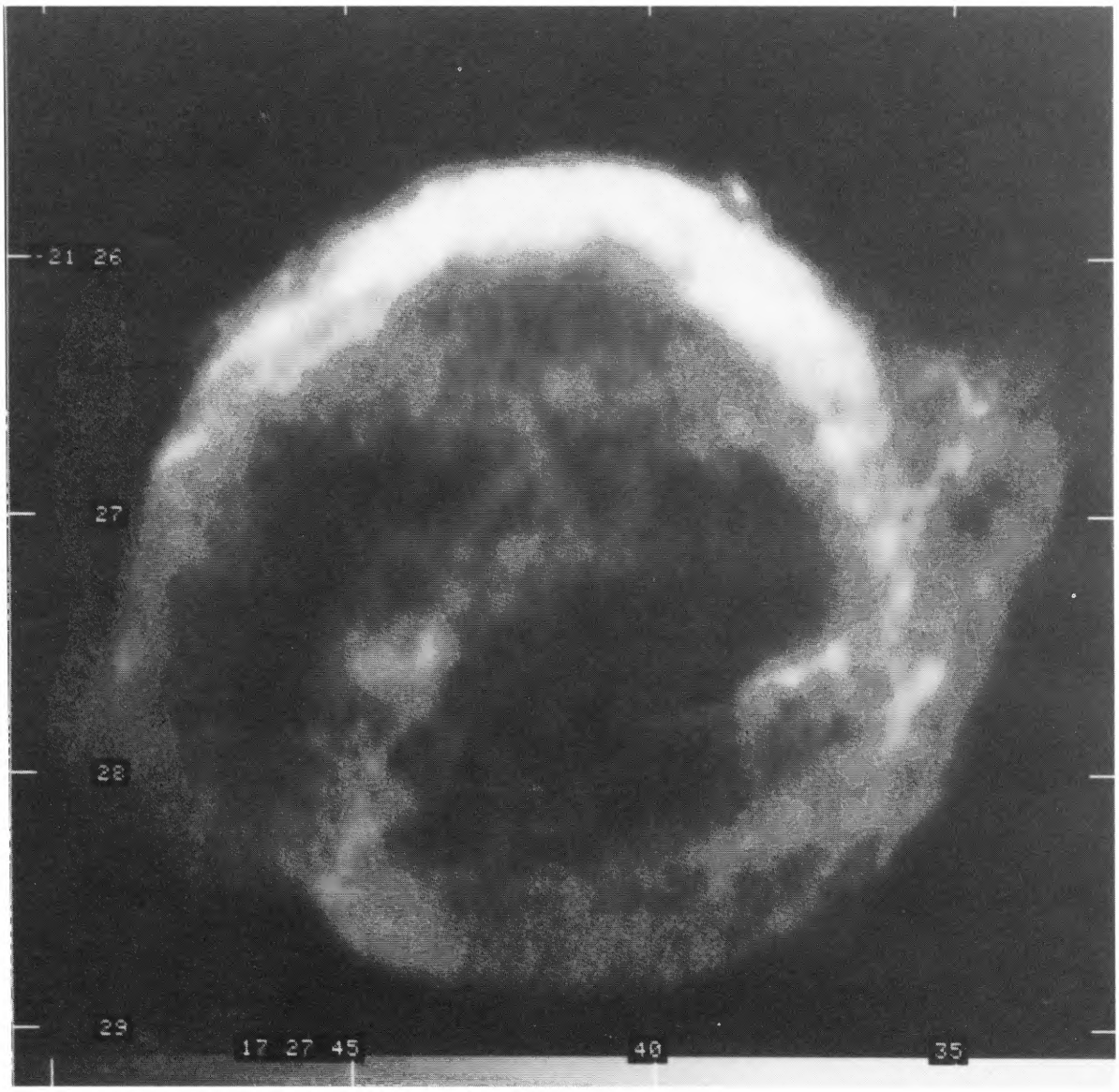

FIG. 1.—20 cm radiophoto of Kepler's SNR. The beamwidth was 2.″72 × 1.′65 with the major axis at a position angle of 0°. The peak surface brightness is 8.16 mJy per beam.

DICKEL *et al.* (*see* **330**, 255)

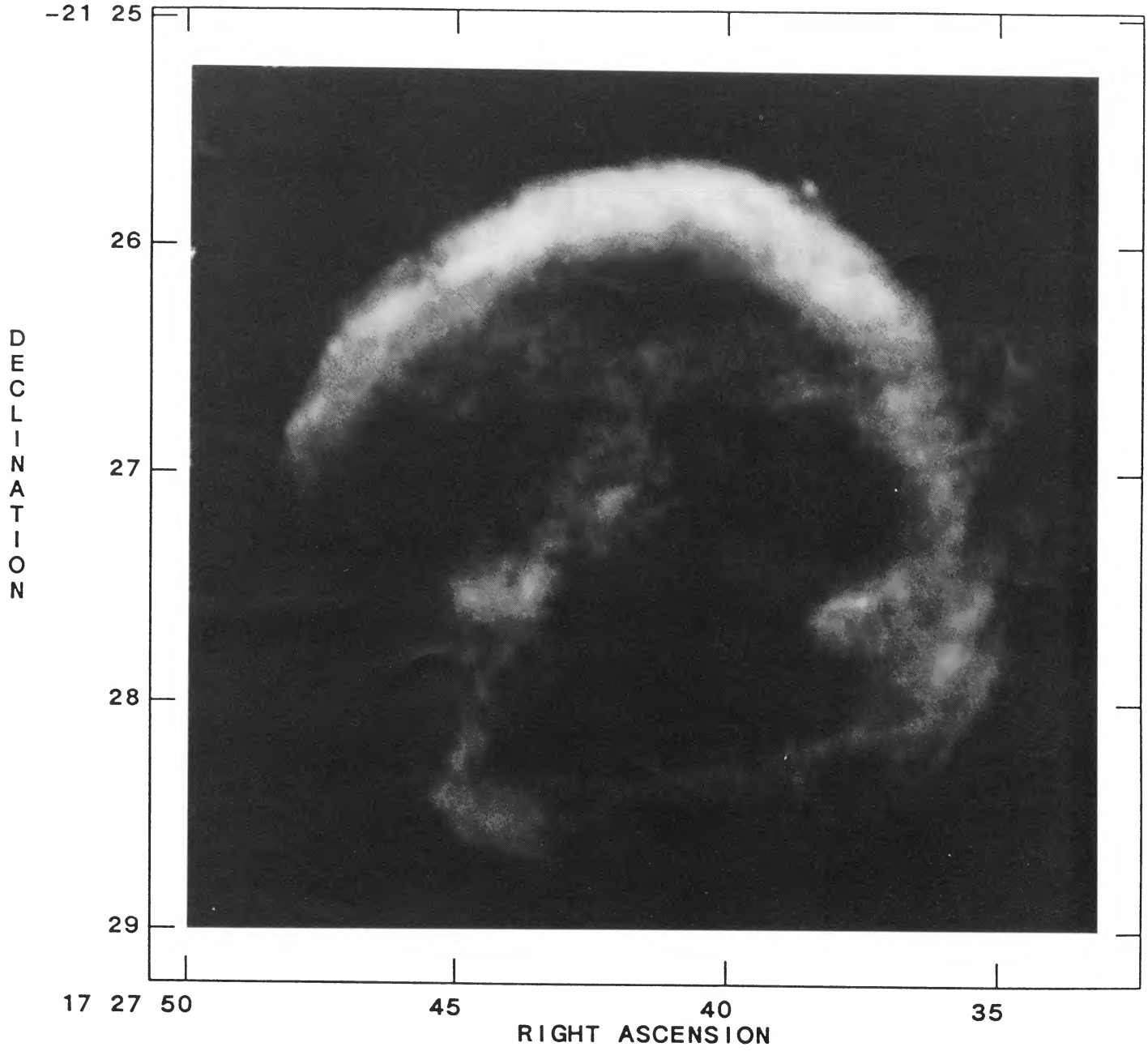

FIG. 2.—6 cm radiophoto of Kepler's SNR. The beamwidth was 0.″93 × 0.″51 with the major axis at a position angle of 0°. The peak surface brightness was 0.37 mJy per beam.

DICKEL *et al.* (*see* **330**, 255)

PLATE 10

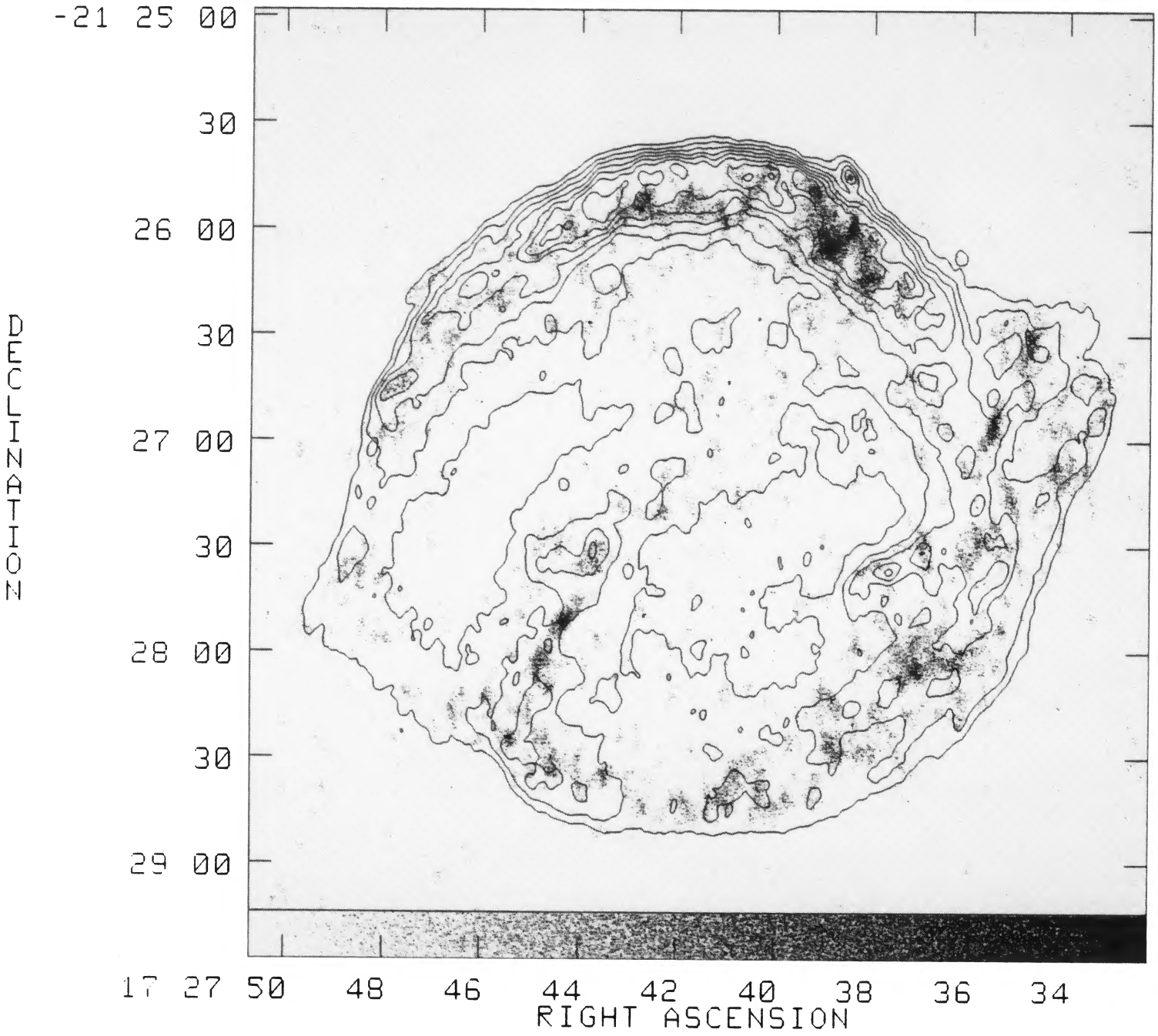

FIG. 3.—Gray-scale representation of the polarized intensity of Kepler's SNR at a wavelength of 20 cm. The gray-scale range goes from 1.2×10^{-4} Jy per beam to 4.2×10^{-4} Jy per beam. Selected contours of the total intensity at values of 1, 2, 3, 4, 5, 6, 7, 8 mJy per beam are superposed.

DICKEL *et al.* (*see* **330**, 255)

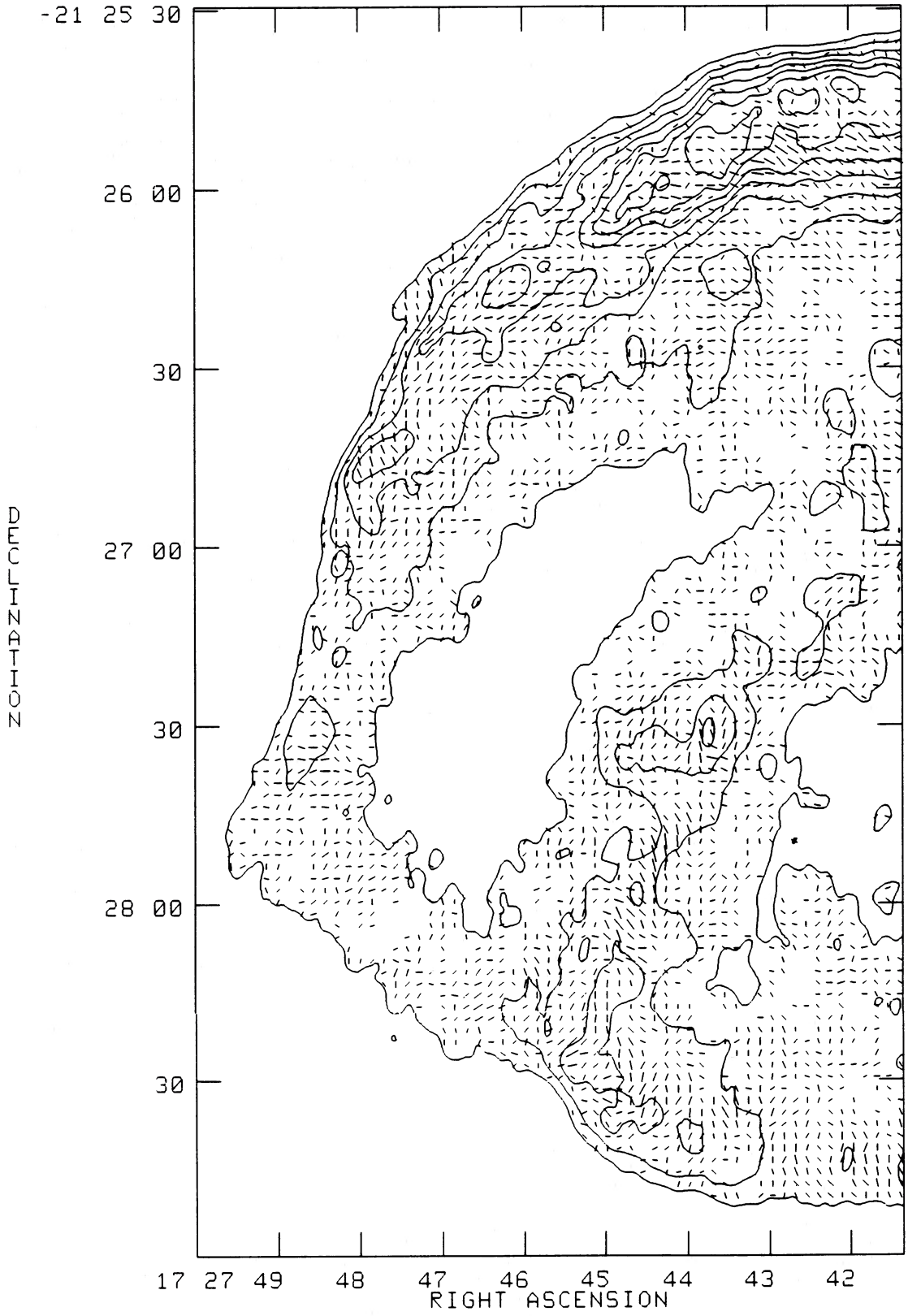

FIG. 4.—The electric vectors of the polarized emission from Kepler's SNR at a wavelength of 20 cm. Only every fourth vector is plotted. A vector length of 1″ corresponds to a polarized flux density of 1.33×10^{-4} Jy per beam. The total-intensity contours have the same values as presented in Fig. 3.

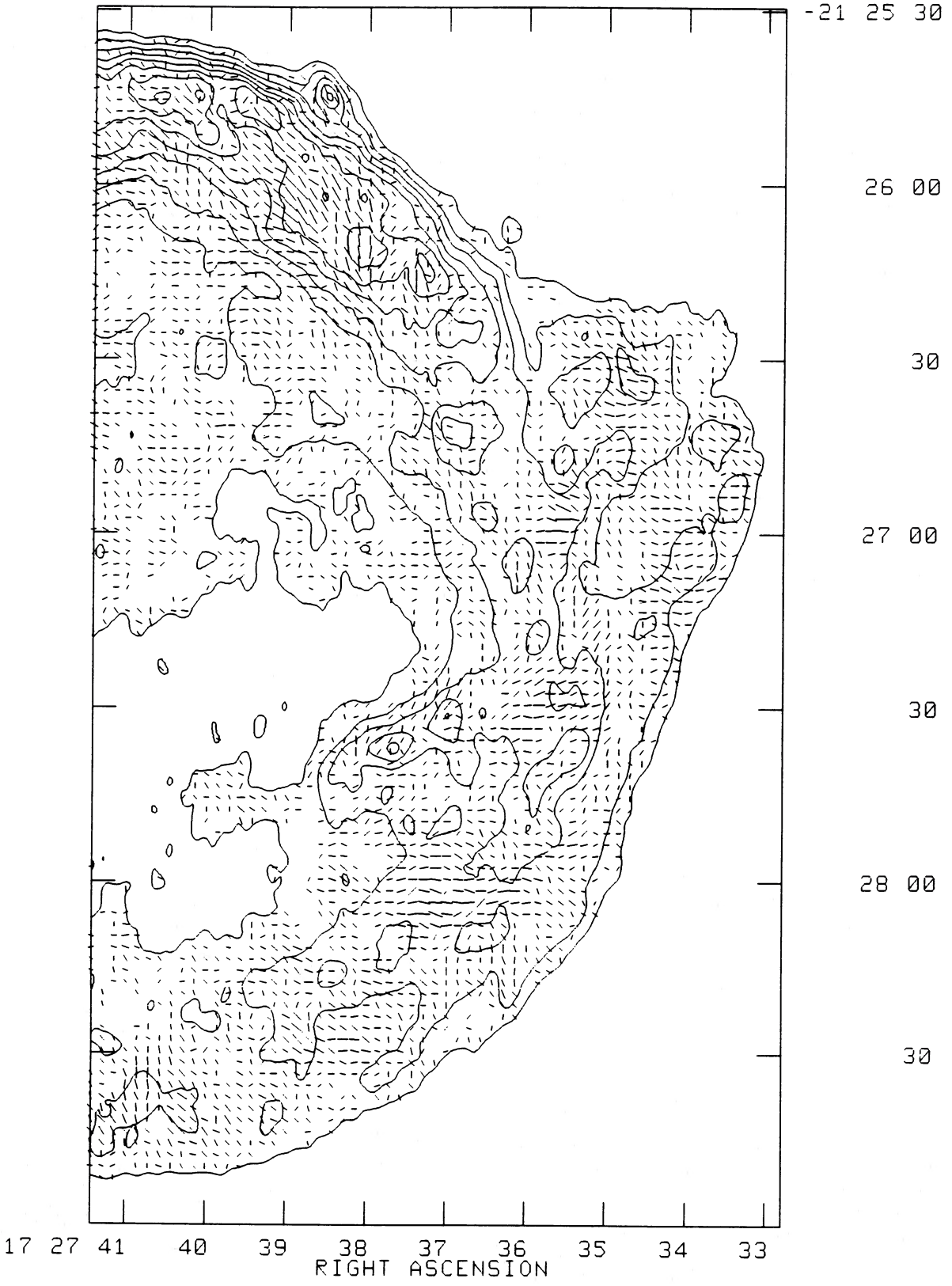

FIG. 4—*Continued*

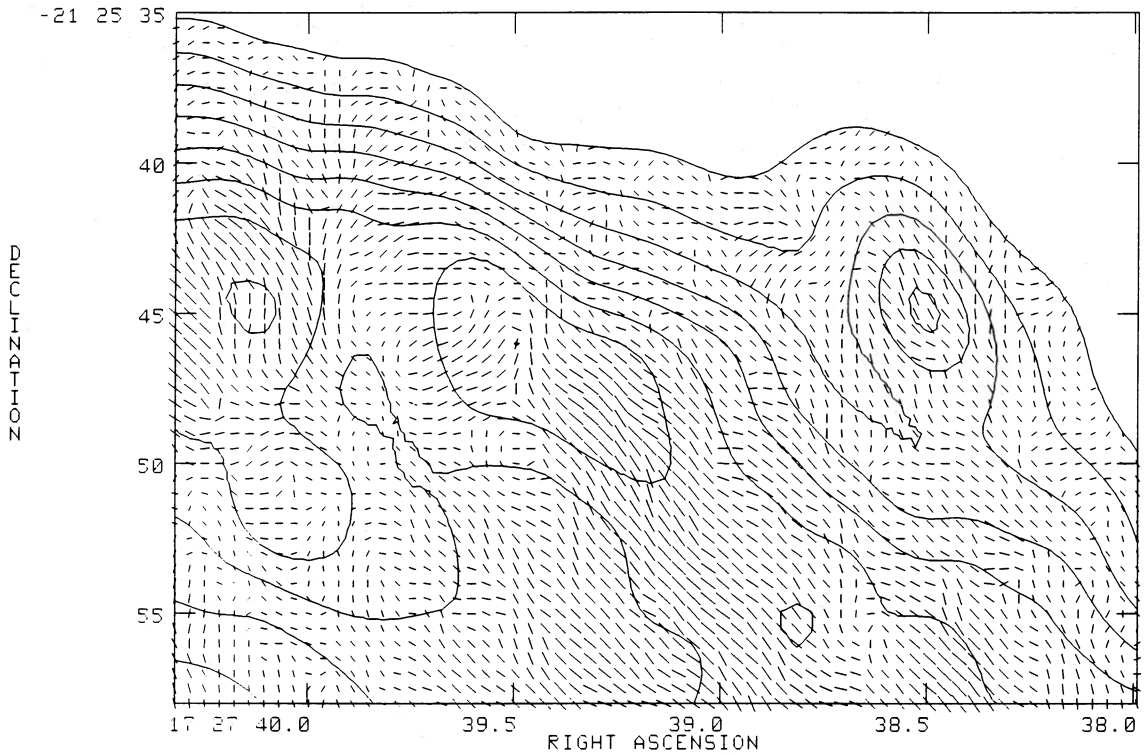

FIG. 5.—Enlargement of the northwest corner of Kepler's SNR showing the electric vector at every grid point. A vector length 1″ corresponds to a polarized surface brightness of 5×10^{-4} Jy per beam. The contours represent the total intensity with the same values as in Fig 3.

b) Data for the Two-Epoch Comparison

Because only the A and C arrays of the VLA were used in 1981, the 1985 maps for the comparative analysis used only data from these same arrays. The mean time interval between the relevant observations was 3.74 yr. The A array interval was 0.2 yr longer and the C array 0.2 yr shorter. The mean interval is 0.98% of the time since the explosion in 1604. For convenience we shall henceforth adopt a value of 1.0% of the lifetime for the interval between maps.

Data from any baseline not present at one epoch because of missing telescopes or other problems were also edited out at the other epoch so that the input data should be as consistent as possible. Occasional delays for individual antenna pairs to come "on line" at the start of a scan or brief dropouts for one or two 30 s integration periods during a scan were not edited so that there were very slight differences in the total numbers of visibility records; at 6 cm there were 201,096 data in 1981 and 201,121 in 1985. The use of uniform weighting for the gridding of the data for the fast Fourier transform used to construct the maps resulted in virtually identical beam patterns at the two epochs. Subtraction of the maps of the two beam patterns at each frequency gave differences which were less than 10^{-6} of the peak brightness, much less than the noise levels on the maps. The maps constructed from the identical data sets also had identical specified parameters. No zero-spacing flux densities were included.

Unfortunately there were no point sources within the field of view of the maps so no direct calibration could be obtained. The chosen calibrator source, 1748−253, was less than 10° from Kepler's SNR and was observed between each scan. Its measured flux density relative to 3C 286 varied randomly within a peak range of 8% over the entire $4\frac{1}{2}$ yr period of the observations. The source 3C 286 is the standard VLA calibrator with no apparent variation greater than 1% so that the fluctuations must be attributed to measurement errors or charges in 1748−253. We conservatively adopt the value of 8% as the uncertainty in any total brightness variations of Kepler's SNR.

III. RESULTS

a) Maps Constructed from the Complete Data Sets

i) *Total Intensity*

These images of Kepler's SNR do not add many new details to our overall view of the object. The short-spacing data from the D array do add a smooth component to the overall level of the remnant and fill in the center to provide a more true representation of the emission from that region. The mean brightness in the center is about one-fourth that of the shell. The pronounced asymmetry in brightness between the northern and southern sides of the remnant has a mean ratio of about 3.

The increased sensitivity to small-scale structure shows that the emission is not all smooth. Brightness contrasts of about 20% are present over a range of sizes in the shell. Although a power spectrum analysis revealed no characteristic length, the mean spacing between bright spots appear to be roughly 10″, about one-half the shell thickness. At a distance of 5 kpc this corresponds to a linear spacing of $\frac{1}{4}$ parsec. All features appear to be larger than a few arcsec; there is no unresolved structure. The long ridges running up the western side of the remnant are more prominent in these maps than in those made previously but they are present in the earlier images and appear to have a thickness comparable to other features.

The leading edge of the shell, although sharp, also appears to be resolved. At the steepest point on the northern side the rise

to half the mean shell brightness occurs in about 3″.6 ≈ 0.09 pc ≈ 2.7×10^{17} cm. In addition, this edge is not perfectly smooth. It exhibits a ripple with a wavelength comparable to the spacing between bright spots on the shell and indentations of perhaps 1″. While the irregularities make it difficult to derive accurate values, the radius of curvature of the fainter southern rim appears to be perhaps 1.1 times that of the bright northern rim.

The radio image appears similar to the X-ray one. When averaged over 30° pie-shaped sectors the data showed a correlation between the radio and X-ray surface brightnesses (MLDG). With the high sensitivity of the current data we have been able to make a higher resolution comparison of the emission in each wavelength band. This is plotted in Figure 6. The axes are linear and were cut off at lower limits near the level of the background. Thus all of the points should be real but the faint ones will be noisy. There are two features which can be readily seen in this picture. First there appears to be a dearth of points near the top right such that the brightest radio emission does not match the brightest X-ray. This is also obvious from inspection of the maps (MLDG); the brightest radio emission is on the north whereas the brightest X-ray patch is in the northwest and somewhat inside the main arc. Second is the significant result that the correlation between the X-ray and radio emission is not very tight. While there are problems with counting statistics at low X-ray surface brightness, it should be noted that the scatter appears to increase at higher surface brightnesses, even at levels where there should be enough photons. In addition we have convolved the images with Gaussian distributions up to 12″ in half-power width and the scatter remains. As a final attempt to detail any specific correlation, we have divided the maps into concentric circles around the remnant and compared the data in each ring separately. This should allow separation of the outer rim, which probably represents the leading shock, from the contact between the ejected and swept-up material further inside, etc. Although the rim region shows a slightly flatter slope, the difference is not statistically significant and the scatter remains large for each ring. We thus conclude that, although there is a global correlation, changes in magnetic field and particle acceleration occur on small scales throughout the remnant and they do not appear to be tied directly to the density of thermal particles so that the relation between the X-ray and radio-emissivity functions is highly variable.

The radio spectral index is another quantity of interest but it is difficult to evaluate from these aperture-synthesis maps because of the response to different spatial-frequency components at each wavelength. To minimize this effect new maps were constructed at each wavelength using only the B array at 20 cm and only the less extended C array at 6 cm. Although there were still some differences in the available spatial-frequency tracks, each map represented a similar range of scale sizes. No zero-spacing flux density was specified at either wavelength. On the bright northern rim where the signal-to-noise ratio is good the spectral index is −0.65 with rms variations of 0.05. The southern part of the shell is considerably fainter and

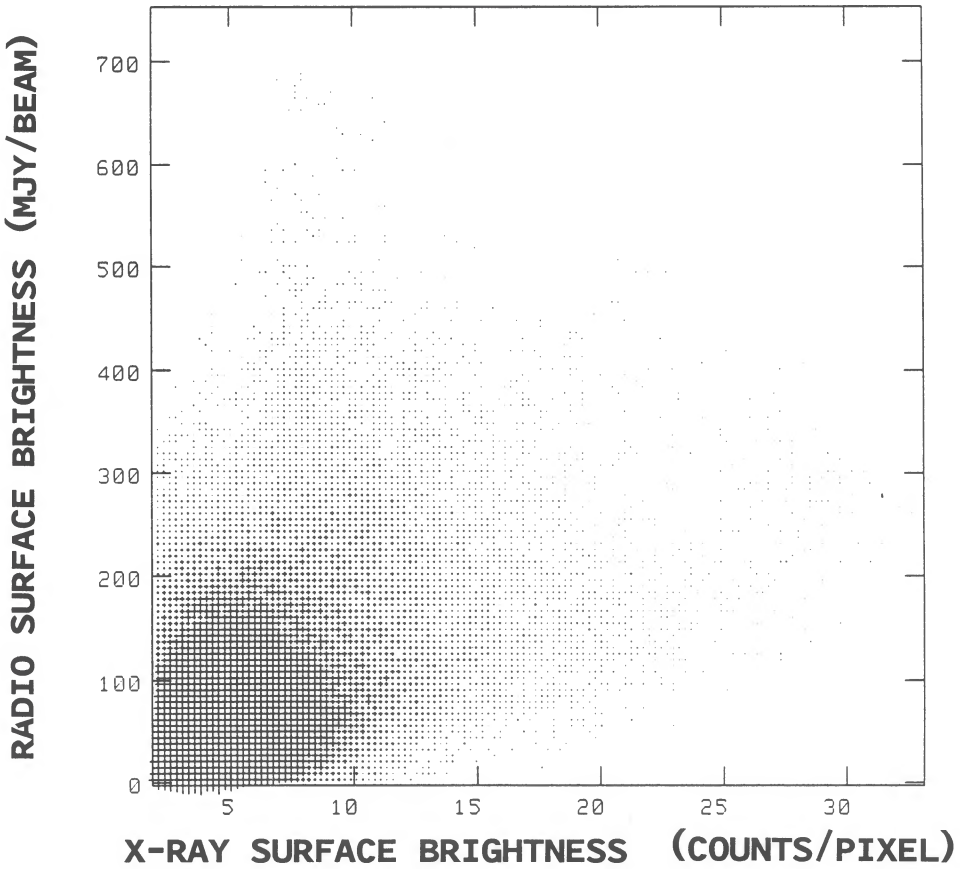

FIG. 6.—Comparison of the 20 cm radio and HRI X-ray surface brightness of Kepler's SNR. Both data sets have been convolved with 3″ Gaussian response functions before comparison. The graph has been divided into 128 cells along each axis, and the size of the cross is proportional to the number of points per cell.

the noise level of the spectral index increases significantly there. Within the noise there is nowhere any indication of a change in spectral index across Kepler's SNR.

ii) *Polarization*

There are clear variations in polarization around the remnant. The high sensitivity to a large range of spatial frequencies has revealed that the position angle appears to have a cellular structure with a size greater than 2″–3″ (Figs. 4 and 5). As for the total intensity, there appears to be a range of cell sizes with no specific size predominating. This phenomenon is similar to that seen in Tycho's SNR (e.g., Strom and Duin 1973). Although noisy, the 6 cm results show the same cellular effect and also confirm the generally small Faraday rotation found by MLDG. The net orientation of the electric vectors is tangential (radial magnetic field) but many individual cells show significant deviations from the net pattern.

The polarized intensity is also not uniform. It fluctuates on a similar scale but is not necessarily correlated with the position angle variations. In addition the polarized intensity is not correlated with the total intensity as can be seen from Figure 7. We not that the polarized intensities are uncorrected for noise in the figure. For analysis, the polarized intensities have been statistically corrected by the maximum likelihood formula given by Simmons and Stewart (1985) and by Killeen, Bicknell, and Ekers (1986). This correction factor differs somewhat at low surface brightness from one given by Wardle and Kronberg (1974) and all values below about 160 mJy per beam are very uncertain. Where the total brightness is greater than 2 mJy per beam the polarized brightness appears to be randomly distributed within a somewhat ragged envelope of roughly constant brightness. The mean fractional polarization appears to decrease from greater than 0.03 in areas with a total surface brightness of 1 mJy per beam to about 0.02 in the brightest regions of the remnant. We also note that the overall fractional polarization is somewhat lower on the bright northern arc and eastern side of Kepler's SNR than on the remaining fainter parts of the remnant. In addition, there is a distinct tendency for the greatest polarized intensity to lie inside the brightest ridge of total emission in the north.

It is also of interest to see if the smooth component to the emission has different polarization properties than the fine-scale features. Comparison of the map from the full data set with that from the A and C arrays alone reveals no position angle variations greater than a noise level of $\pm 20°$ (or less at high brightness levels). The polarized surface brightnesses are fairly noisy as described above but they are correlated on the two different-resolution maps and there is no indication of any differences between them. Thus the observed cell size appears to dominate the polarization structure. The polarization is probably controlled more by the dynamics of the expansion than by the mechanisms enhancing the radio emission. Expansion of the remnant into a clumpy medium will result in many Rayleigh-Taylor unstable interfaces which will tend to provide a cellular pattern and also increase the polarization with a net radial orientation for the magnetic field as observed.

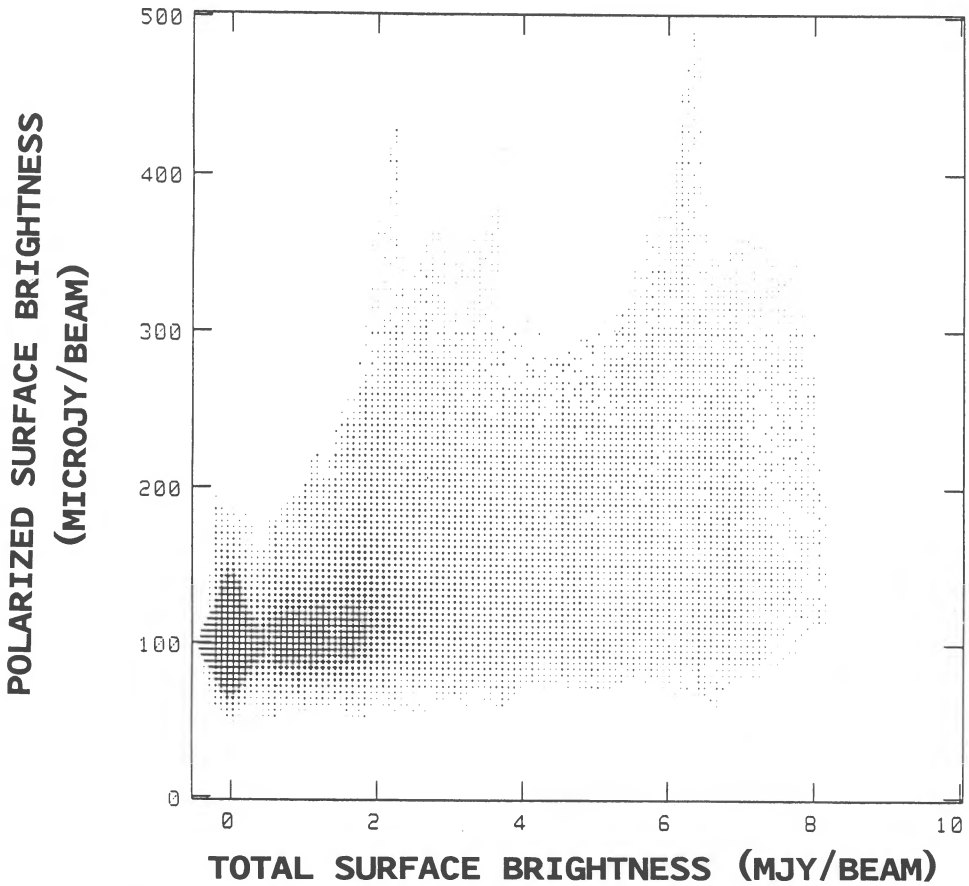

FIG. 7.—Comparison of the polarized and total surface brightnesses of Kepler's SNR at a wavelength of 20 cm. The graph has been divided into 128 cells along each axis and the size of the cross is proportional to the number of points per cell. The polarized surface brightnesses in this plot are uncorrected for noise.

b) Comparison of the 1981 and 1985 Results

To measure the expansion and possible brightness change of Kepler's SNR between 1981 and 1985, we adopted a technique similar to that proposed by Tan and Gull (1985). The procedure varies parameters, such as expansion, so as to maximize a maximum-likelihood criterion. The process can be viewed as adjusting parameters of one map to make it "fit" the other, and so the residuals of the fit are the quantities of interest.

Although we do not expect the center of the remnant to have moved significantly in the 4 yr time interval, there could be slight apparent positional changes due to calibration errors or changes in differential refraction between the calibration source and Kepler's SNR because of atmospheric variations. Also, any changes in amplitude of components which are missing from the limited spatial-frequency coverage of these aperture-synthesis observations could cause small differences in the bias of the zero level of the two maps. Thus the final solutions allowed for variations of five parameters: expansion, which is the ratio of the radial distance from the center of the remnant of the brightness distribution in 1985 to that in 1981; amplitude, which is the mean ratio of the surface brightness in 1985 to that in 1981; right ascension shift; declination shift; and offset, which is a shift in the zero level of the surface brightness. It should be noted that this solution is by nature intensity weighted so that it measures the whole shell and not just the outer rim of the SNR.

The analysis procedure met with somewhat limited success because of (*a*) the low signal-to-noise ratio of the data, (*b*) the fact that the change in size was near the resolution limit, and (*c*) differences in both the expansion and the brightness change at different positions in the remnant. All of these characteristics tended to produce several local minima in a rather flat solution space rather than a single sharp minimum. Attempts to taper the raw spatial-frequency data or smooth the final maps for increased signal-to-noise ratio reduced the sensitivity to the small angular scales where the difference is most significant. The current radius of the remnant is about 100″ and the rate of expansion is less than linear in time so that it was necessary to measure changes of less than 1″. Therefore, despite the low surface brightness of Kepler's SNR relative to the noise level, we have used the full resolution maps at 6 cm to evaluate the evolution. Attempts to fit maps with half-power beamwidths greater than 1″ (either smoothed 6 cm or raw 20 cm) found minima near zero expansion but produced residual maps which clearly showed a radial distortion characteristic of faster expansion. In addition, although the spatial frequency coverage was nearly identical in the two cases, the source has changed between the two epochs and because of the sparcity of the data, the variation in sidelobe patterns can affect the maps differently. These significant negative and positive patterns can distort the solution and certainly make the residual map noisy. Thus the final solution has been done with maps which have been deconvolved by the maximum-entropy technique to produce images which were least contaminated by the instrumental pattern.

The result gave a mean expansion of 1.0050 times the original size which corresponds to an expansion parameter $x = 0.50$ (recall that radius is proportional to time to the x power). The mean surface brightness decreased to 0.99 of its initial value, the right ascension and declination shifts were $\Delta\alpha = 0\overset{s}{.}1$ and $\Delta\delta = 0''.2$, respectively, and the offset was 10^{-3} times the peak brightness of the maps. The residual map in Figure 8 (Plate 11) which corresponds to 1985 minus 1981 expanded and adjusted by the best-fit parameters had rms fluctuations of about 0.06 times the peak brightness of the original maps; this was about $2^{1/2}$ times the rms noise level on each original map as expected for a correct fit.

Several additional fits were made with small differences to the inputs. These included fixing the right ascension and declination shifts to zero, trimming the corners of the maps where there is no emission from the SNR, or using the direct images rather than the maximum entropy results. These modifications gave values for the mean expansion parameters which ranged from 0.49 to 0.56 and amplitude changes between 0.99 and 1.01. The range of these values is larger than the formal errors of fit of the individual solutions and probably represent a reasonable range for the uncertainty in the mean values.

More important than the range of possible solutions is the fact that the residual map shows what appear to be correlated differences from pure noise on several positions around the remnant. A bright outer rim and fainter interior represents faster expansion than the average while a dark rim and brighter interior represents slower expansion. Thus we attribute the observed patterns to actual differences in the expansion and brightness changes. It is difficult to quantify the variations in different directions because they must necessarily be determined over narrow wedges which are very subject to small positional offsets and also to changes in individual features seen on the face of the remnant which may be moving at different projected rates than the overal rim. To find approximate solutions in each direction we have produced a series of residual maps with the expansion parameter fixed at values of 0.30, 0.35, 0.40, 0.45, 0.50, 0.55, 0.60, and 0.65. The best-fitting expansion in each wedge was then chosen by inspection of the residual maps. The values of the expansion factor for the sectors in which they could be reasonably determined are sketched in Figure 8. Each number represents the value of the expansion parameter for the map on which the residual for that sector only was the smallest. We have not refined the values more accurately than the 0.05 increment in x between individual maps. The protuberances in the northwest and southeast corners of the SNR do not appear to be expanding much faster than the rest of the remnant. Although these areas are too faint and irregular to obtain good values of the expansion, a residual map for an expansion parameter of 0.65 clearly shows a black rim arising on the outside which indicates that the expansion parameter must be less than this value and the best estimates are shown in Figure 8.

To assess local brightness changes, the residual map was divided by the 1985 total-intensity map to obtain the fractional variation. The result for the $x = 0.50$ map is shown in Figure 9 (Plate 12). The results for other expansion parameters change the numbers somewhat right at the rim of the remnant but do not modify the overall picture significantly. The northern part of the shell, with the slowest expansion has decreased in brightness by about 5% in 4 yr. Differential changes in other regions cannot be distinguished and are probably less than 2%.

The small diameter source just on the outer edge of the north rim at $\alpha\ 17^{h}27^{m}38\overset{s}{.}51$ and $\delta\ -21°27'44''.0$ is resolved with a size of 6″.0 by 2″.7. It appears to be moving outward with about the mean rate for the whole remnant rather than the slower value of the nearby part of the main shell. It is not changing brightness significantly.

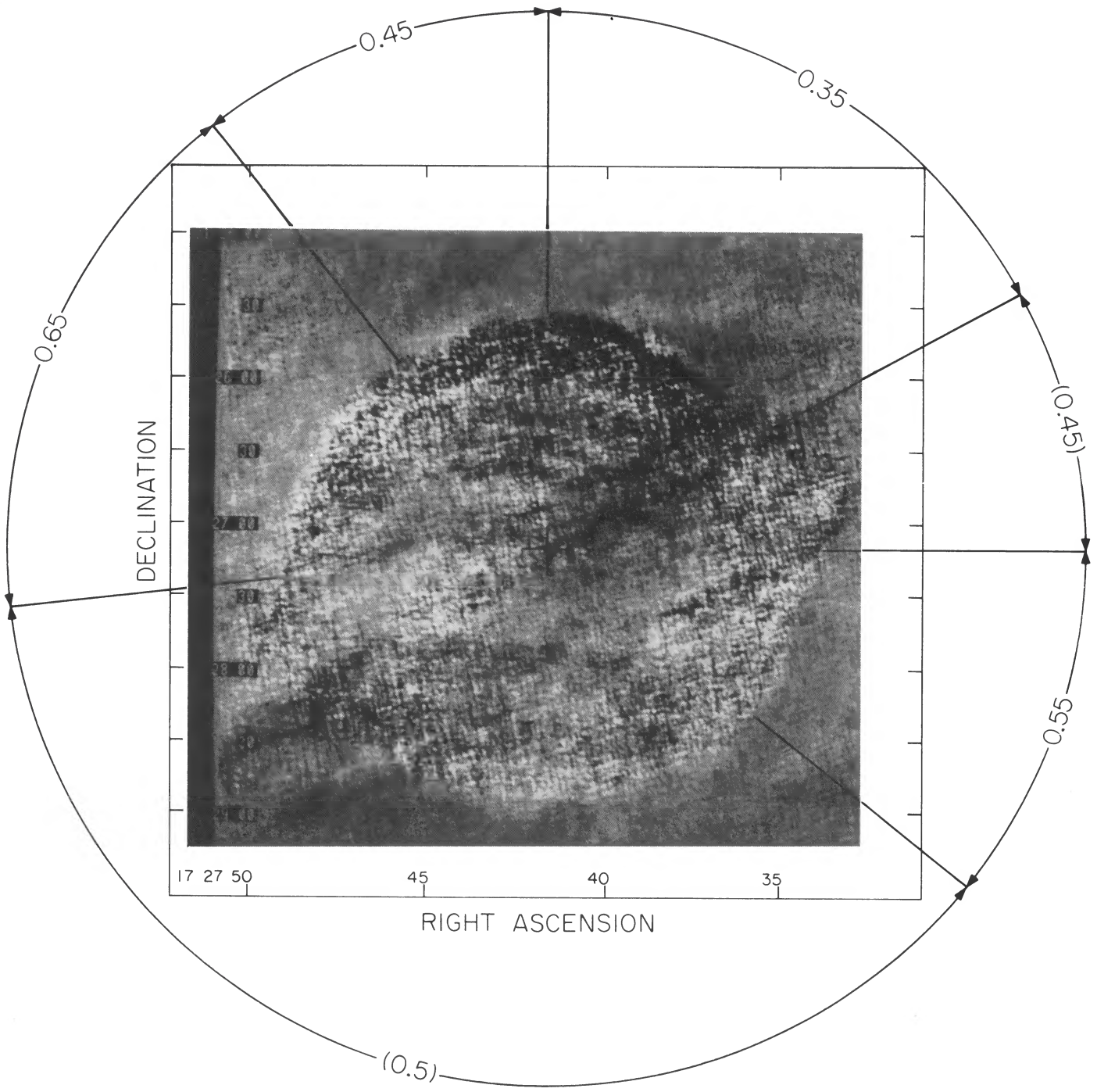

FIG. 8.—Best-fitting residual map for the mean overall expansion of Kepler's SNR between 1981 and 1985. The input maps were made at a wavelength of 6 cm and have been treated with a maximum entropy deconvolution. The map is for the mean expansion factor of 1.0050 corresponding to an expansion parameter $x = 0.50$ for the whole remnant over the 4 yr time interval between observations. There are clear variations among different parts of the remnant, however, and the numbers around the rim represent approximate expansion parameters for the indicated sectors. The boundaries are not as distinct as marked. The values in parentheses are particularly uncertain.

DICKEL *et al.* (*see* **330**, 261)

PLATE 12

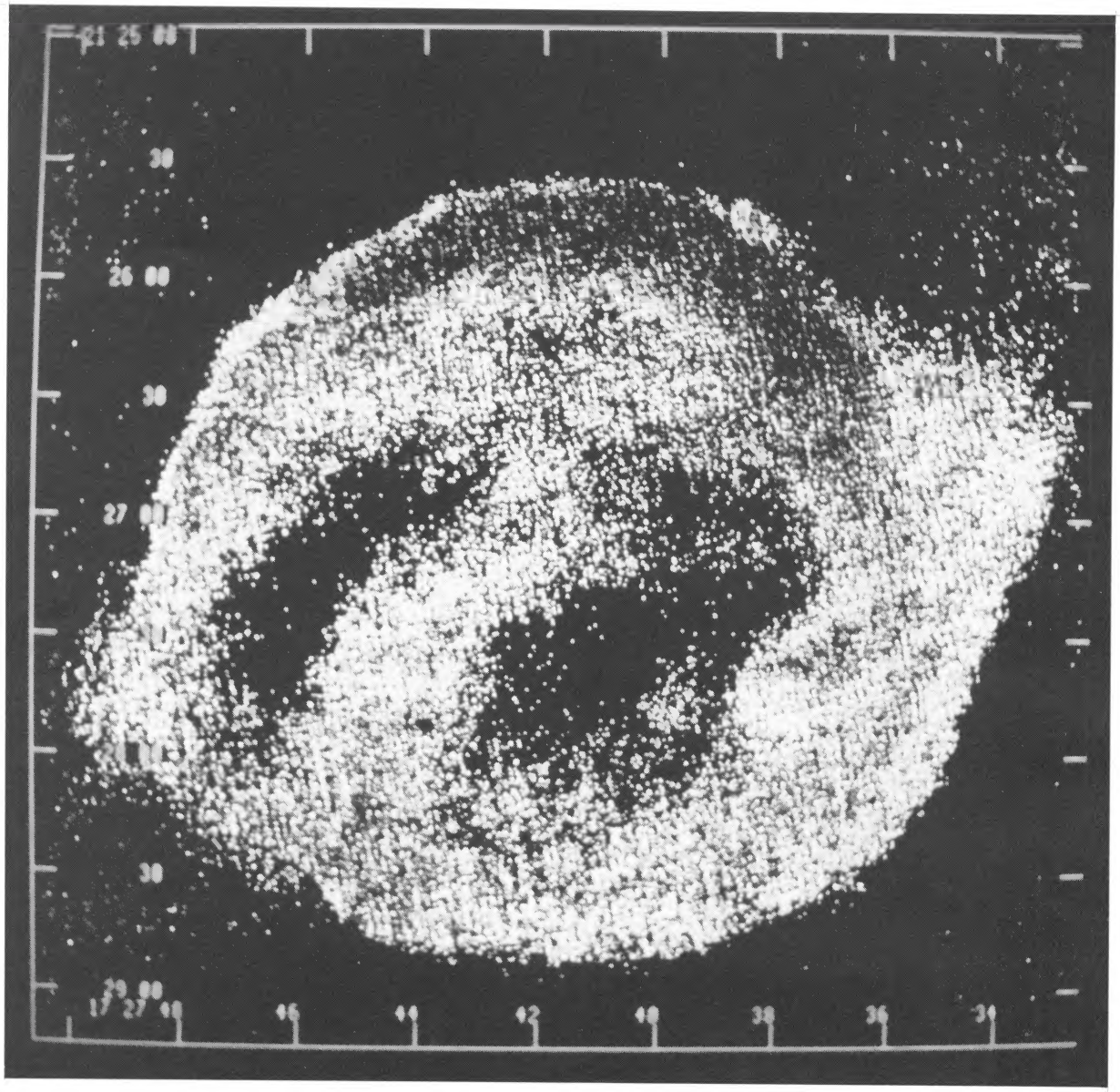

FIG. 9.—Fractional residual map showing the changes between 1981 and 1985 divided by the 1985 map. Relativity dark areas indicate declining brightness. Although the figure is noisy, the general trends are correct. The significant gray-scale range is between -0.2 and $+0.1$.

DICKEL *et al.* (*see* **330**, 261)

IV. DISCUSSION

The complexity of Kepler's SNR when viewed in detail and the lack of tight correlations between observed properties argues for a variety of conditions within the remnant. The brightness pattern fluctuates by more than 20% of the mean value in total intensity and over a considerably larger range in polarized intensity. Some regions appear as random clumps whereas others might be fragments of broken shells. Irregularities in the ambient medium around the star provide an obvious source of variations (Shirkey 1978; Dickel and Jones 1985). They could be either in the general interstellar medium or in material lost by the star before the supernova explosion. The outward shock leading the expansion is at the outer edge of the observable shell and the contact between the ejectum and swept-up material is embedded in this shell. Rearrangement of the magnetic field by passage of the shock through this clumpy medium should give polarization cells.

In addition, as Rayleigh-Taylor instabilities grow (Gull 1973) finger-like structures will develop and stretch away from the boundary. This movement of material should stretch the frozen-in magnetic field in a net radial direction and could account for the increase in polarization on the inner side of the bright northern shell. The lack of such an obvious effect in the south could be a sensitivity problem or perhaps a weaker instability at the contact. As the disturbance grows, pieces may break off and slowly dissipate into the surrounding shocked medium. At first the blobs will not be in equilibrium with their surroundings; as outward moving clumps expand adiabatically, their radio brightness will decrease faster than the field structure. This evolution would be in the correct sense to explain the apparent effect of somewhat higher fractional polarization at lower surface brightness.

Expansion of the young remnant of a presumed Type I SN into an homogeneous medium should result in an expansion parameter for the shell between the forward and reverse shocks of 0.57 (Chevalier 1982) whereas the remnant of a massive progenitor with a steeper exterior density gradient and probably a stellar wind would have a much larger expansion parameter (near 0.9). The observed expansion, however, will not necessarily have exactly either of these values. A given parcel of gas can change the brightness as well as move, thus distorting the apparent shift of a feature and the net sum over the whole shell will tend to be slightly slower than the expansion of the rim. The mean value of the observed expansion parameter of 0.50 is consistent with a low-mass progenitor for Kepler's SNR and shows that the remnant has not yet reached the Sedov phase of its expansion. Braun (1987) has interpolated models presented by Gull (1973) to predict expansion parameters similar to those found and a ratio of swept-up to shocked-ejected material of 5.4. Gull's models, however, used an unrealistic square piston and did not consider the reverse shock moving back into the ejectum. In the current Chevalier phase with a more realistic physical model the ratio of swept-up to shocked-ejected mass is 2 (Chevalier 1982). This value might remove some of Braun's difficulty of needing a reasonably large fraction of mass tied up in dense knots which are not part of the expanding flow.

If the total shocked mass is less than 2 $M_\odot$ (White and Long 1983) then less than 0.67 $M_\odot$ of ejected matter has been encountered by the reverse shock which should have moved about half way back into the stellar material. The change between the Chevalier and Sedov phases is very quick so that if the observed expansion parameter represented a moment in the transition for a massive progenitor it would need to be very near the Sedov phase and the shocked mass should be much greater than observed.

There are certainly deviations on small scales from the mean changes in the remnant with time. As density enhancements in the surrounding medium are encountered, the expansion should be slowed temporarily and the brightness will be higher. Model calculations for a clumpy medium give significant fluctuations in the observed expansion parameter at different positions in the shell. The fact that the extended protuberances are currently expanding at the average rate might suggest that the expansion encountered little material in those directions at early times and that the density has remained reasonably uniform.

The northern side of Kepler's SNR is the brightest and appears to be expanding the least rapidly. This section also appears to be decreasing in brightness with time relative to the rest of the remnant. These phenomena can be explained by an increase in the swept-up mass on the northern side. At first the brightness in dense areas will be greater but as the energy is used up and the shock slows, the brightness will decrease faster than in less dense regions. A mean density-increase of about a factor of $1\frac{1}{2}$ can produce the observed difference. Whether this is caused by a general gradient in density from south or north or a specific density increase encountered since the explosion cannot be determined, however. Obtaining a unique answer for the density distribution will require continued monitoring of the remnant over several tens of years to determine the actual acceleration/deceleration of the expansion and the rate of change of the brightness changes. An interval of about 10 yr is probably sufficient for this purpose.

We thank Knox Long and Eric Greisen for advice in the early phases of this research. Many discussions with Eric Jones are greatly appreciated. The effort was supported, in part, by NASA grant NAG8-540. J. R. D. acknowledges the support of the Earth and Space Science Division of the Los Alamos National Lab while he was on sabbatical there.

REFERENCES

Bell, A. R. 1977, *M.N.R.A.S.*, **179**, 573.
Braun, R. 1987, *Astr. Ap.*, **171**, 233.
Chevalier, R. A. 1982, *Ap. J.*, **258**, 790.
Dickel, J. R., and Greisen, E. W. 1979 *Astr. Ap.*, **75**, 44.
Dickel, J. R., and Jones, E. M. 1985, *Ap. J.*, **288**, 707.
Dickel, J. R., Jones, E. M., and Eilek, J. A. 1987, in *The Origin and Evolution of Neutron Stars*, ed. D. J. Helfand and J. H. Huang (Dordrecht: Reidel), p. 126.
Gull, S. F. 1973, *M.N.R.A.S.*, **161**, 47.
Kamper, K. W., and van den Bergh, S. 1978, *Ap. J.*, **224**, 851.
Killeen, N., Bicknell, G. V., and Ekers, R. D. 1986, *Ap. J.*, **302**, 306.
Matsui, Y., Long, K. S., Dickel, J. R., and Greisen, E. W. 1984, *Ap. J.*, **287**, 295 (MLDG).
Sedov, L. 1959, *Similarity and Dimensional Methods in Mechanics* (New York: Academic Press).
Shirkey, R. C. 1978, *Ap. J.*, **224**, 477.

Simmons, J. F. L., and Stewart, B. G. 1985, *Astr. Ap.*, **142**, 100.
Strom, R. G., and Duin, R. M. 1973, *Astr. Ap.*, **25**, 351.
Strom, R. G., Goss, W. M., and Shaver, P. A. 1982, *M.N.R.A.S.*, **200**, 473.
Tan, S. M., and Gull, S. F. 1985, *M.N.R.A.S.*, **216**, 949.
Tuffs, R. 1984, Ph.D. thesis, University of Cambridge.
van den Bergh, S., and Kamper, K. W. 1977, *Ap. J.*, **218**, 617.
———. 1983, *Ap. J.*, **268**, 129.
Wardle, J. F. L., and Kronberg, P. P. 1974, *Ap. J.*, **194**, 249.
White, R. L., and Long, K. S. 1983, *Ap. J.*, **264**, 196.

RICHARD G. ARENDT, JOHN R. DICKEL, and ROBERT SAULT: 349 UI Astronomy Bldg., 1011 West Springfield, Urbana, IL 61801

KIRK T. KORISTA: Astronomy Department, Ohio State University, 174 West Eighteenth, Columbus, OH 43210

YUTAKA MATSUI: Physics and Astronomy Department, Northwestern University, 2145 Sheridan Road, Evanston, IL 60601